J. Fluid Mech. (1994), *vol.* 266, *pp.* 319–346

Rotating axial flow of a continuously separating mixture

By A. A. DAHLKILD AND G. AMBERG
Department of Mechanics, Royal Institute of Technology, 100 44 Stockholm, Sweden

(Received 19 January 1993 and in revised form 16 September 1993)

We consider the continuous separation process of a monodispersed suspension flowing axially through a rotating circular cylinder. This stationary problem can be regarded as a basic flow case of rotating mixtures in conjunction with previous studies of time-dependent flows like spin-up and batch settling in a cylinder. The 'mixture model' for two-phase flow is used to formulate the problem, which is solved in the range of small Ekman and Rossby numbers by asymptotic analytical methods and by a numerical code. The gradual separation of the axially injected suspension is manifested as a stationary stratification of the mixture which induces a swirl component of the velocity, in analogy with the thermal wind in the Earth's atmosphere. The presence of the azimuthal motion and induced secondary flow due to Ekman-layer pumping clearly influences the character of the stratification. Analytical and numerical results are in excellent agreement.

1. Introduction

Within the theory of rotating mixtures several basic, time-dependent flow fields have been considered in the literature. In a majority of those papers a homogeneous monodispersed suspension of spherical particles is at an initial instant assumed to be at rest relative to a rapidly rotating container. The subsequent time-dependent separation process has been studied in some detail. A selection of these papers is briefly mentioned here. Batch separation in an infinite circular cylinder was studied by Greenspan (1983) and Schaflinger & Stibi (1987) and the effect due to a finite cylinder was investigated by Ungarish (1986, 1988*a*). Geometrical enhancement of centrifugal separation due to inclined endcaps was investigated by Greenspan & Ungarish (1985*a*), Amberg *et al.* (1986) and Ungarish (1988*b*). The effect of meridional barriers on batch separation in various geometries was studied by Greenspan & Ungarish (1985*b*), Schaflinger, Köppl & Filipczak (1986), Schaflinger (1987), Amberg & Greenspan (1987), Greenspan (1988) and Dahlkild & Greenspan (1989). The spin-up from rest of a mixture in a straight cylinder was analysed by Ungarish (1990, 1991) for the cases of heavy and light particles and by Amberg & Ungarish (1993) for light particles. The most recent review on centrifugal separation is given by Schaflinger (1990), to which the reader is referred for a thorough study on the subject. Fundamentals of separation are also given in a textbook by Ungarish (1993) where much of the work referred to above is treated.

In industrial applications centrifugal separation is often a stationary process where the mixture is fed into the separator and the separated products collected continuously. Amberg *et al.* (1986) considered the continuous separation of a dilute suspension in the narrow gap between the conical plates of an industrial centrifugal separator, and this seems to be one of the few theoretical studies on continuous centrifugal separation of

a two-phase mixture from first principles of fluid dynamics. Dahlkild, Amberg & Greenspan (1992) analysed the continuous flow in a centrifugal spectrometer, but only traced single sedimenting particles in a single-phase flow field.

Experiments on centrifugal separation problems are rare, probably owing to the technical difficulties of making measurements in two-phase flows. Of the studies mentioned above only the paper by Schaflinger *et al.* (1986) presents quantitative experimental results. Otherwise only visual demonstrations are presented by the authors, which nevertheless give an illustrative qualitative verification of the analysis, as, for example, Amberg & Greenspan (1987) and Ungarish (1991).

The objective of the present work is to complement the very few analytical studies on continuous separation processes. We study here the centrifugal separation of a mixture, continuously fed at the bottom of a circular cylinder and led axially towards the outlet at the top. The problem is sufficiently simple to allow an analytical study but at the same time it contains several basic features of a stationary separation process.

A special feature is the analysis of the Ekman layers which appear at boundaries with either suction or injection of fluid. There seem to be no linear theories available in the literature for such flows, but von Kármán's (1921) similarity solution of the fully nonlinear flow over a rotating disk has been extended by several authors to include the effects of suction or injection at the disk. Stuart (1954) considered the case of strong suction at a rotating disk and obtained a series solution in powers of the inverse suction parameter. Rogers & Lance (1960) obtained numerically computed similarity solutions in the case of suction at a rotating disk with the fluid also rotating far away from it at a different speed. Additional aspects of flow over a rotating disk with suction or injection and the fluid non-rotating at infinity have been treated by various authors (see e.g. Goldshtik & Javorsky 1989). However, to obtain the oscillating behaviour typical of Ekman layers it is necessary for the fluid to be rotating far away from the disk also. In contrast to the nonlinear similarity solutions discussed above the approach here is a straightforward linear boundary-layer analysis in which the velocity component normal to the boundary, representing the injection or suction of fluid, are approximately constant through the boundary layer. As the strength of the suction/injection is of the same order of magnitude as the tangential velocity difference between the boundary and the fluid far away from it, convection of momentum in the direction normal to the boundary are significant. The secondary Ekman pumping effect is reconsidered accordingly. These results for the Ekman layer are of a general nature and not restricted to two-phase flow applications.

There is also an urgent need for numerical prediction of two-phase flow fields, especially in the light of the experimental difficulties. Commercial computer codes are at hand but the output can be difficult to interpret without very detailed knowledge of the software and long experience of running the code. To obtain confidence in a two-phase code, verification of the results in cases where an analytical solution is tractable for comparison is especially important, since models of two-phase flow vary and can even be unsatisfactory. For the case of spin-up from rest of a mixture of light particles, Amberg & Ungarish (1993) obtain good agreement between the analytical and numerical solutions of the 'mixture model' equations for two-phase flow (see Ishii 1975). In our work their code is slightly modified to deal with the continuous separation process studied here, the outcome of which constituted an additional successful test of the code.

2. Formulation

Centrifugal separation of a mixture, consisting of a Newtonian liquid phase and a dispersed phase of spherical particles, all with the same radius a^*, is assumed to take place in a straight circular cylinder of radius r_0^* aligned with the rotation axis $\boldsymbol{e}_z$ as sketched in figure 1. At the bottom of the cylinder, rotating at angular velocity Ω^*, a homogeneous mixture is uniformly injected and at the top, a distance H^* above the bottom, partially separated mixture and fluid are ejected at the same volumetric flow rate. In the mathematical formulation we utilize the 'mixture model' of two-phase flow (see Ishii 1975) where the mixture is treated effectively as a single Newtonian fluid. The mass-averaged velocity of the mixture denoted by $\boldsymbol{q}^* = (u^*, v^*, w^*)$ should be distinguished from the volume-averaged velocity $\boldsymbol{j}^* = (j_r^*, j_\theta^*, j_z^*)$ where the coordinate directions $(\boldsymbol{e}_r; \boldsymbol{e}_\theta; \boldsymbol{e}_z)$ are shown in figure 1. Variables of the continuous and dispersed phases are denoted by subscripts C and D respectively. The relative velocity between the phases is given by

$$\boldsymbol{q}_R^* = \boldsymbol{q}_D^* - \boldsymbol{q}_C^*. \tag{2.1}$$

If the particle volume fraction is α, the mixture density is then

$$\rho^* = \alpha\rho_D^* + (1-\alpha)\rho_C^*. \tag{2.2}$$

The effective mixture viscosity was assumed to be an empirically determined function of the particle concentration of the form

$$\mu^* = \mu_C^* \mu(\alpha). \tag{2.3}$$

Here we use

$$\mu(\alpha) = (1-\alpha/\alpha_M)^{-2.5\alpha_M}, \quad \alpha_M = 0.66. \tag{2.4}$$

Variables are non-dimensionalized according to

$$\boldsymbol{r} = \frac{\boldsymbol{r}^*}{r_0^*}, \quad t = t^*|\epsilon|\beta\Omega^*, \quad \boldsymbol{q}_R = \frac{\boldsymbol{q}_R^*}{|\epsilon|\beta\Omega^* r_0^*}, \quad \boldsymbol{q} = \frac{\boldsymbol{q}^*}{Ro\,\Omega^* r_0^*}, \quad P = \frac{P^*/\rho_C^*(\Omega^* r_0^*)^2 - \frac{1}{2}r^2}{Ro}, \tag{2.5}$$

where non-dimensional quantities are without asterisks. P is here the non-dimensional reduced pressure. The relative density difference ϵ and the particle Taylor number β are dimensionless parameters defined by

$$\epsilon = \frac{\rho_D^* - \rho_C^*}{\rho_C^*}, \quad \beta = \frac{2}{9}\frac{a^{*2}\Omega^*}{\nu_C^*}. \tag{2.6}$$

and the Rossby number Ro will be specified later. Useful relationships between the mass- and volume-averaged velocities are given by

$$\boldsymbol{j}_D = \alpha\boldsymbol{j} + \frac{|\epsilon|\beta}{Ro}\alpha(1-\alpha)\boldsymbol{q}_R, \tag{2.7}$$

$$\boldsymbol{j} = \boldsymbol{q} - \epsilon\frac{|\epsilon|\beta\alpha(1-\alpha)}{Ro(1+\epsilon\alpha)}\boldsymbol{q}_R. \tag{2.8}$$

The stationary equations of mixture theory in a coordinate frame $(\boldsymbol{e}_r; \boldsymbol{e}_\theta; \boldsymbol{e}_z)$ rotating with the cylinder are, for conservation of mixture and dispersed-phase volume,

$$\nabla\cdot\boldsymbol{j} = 0, \tag{2.9}$$

$$\nabla\cdot\boldsymbol{j}_D = 0, \tag{2.10}$$

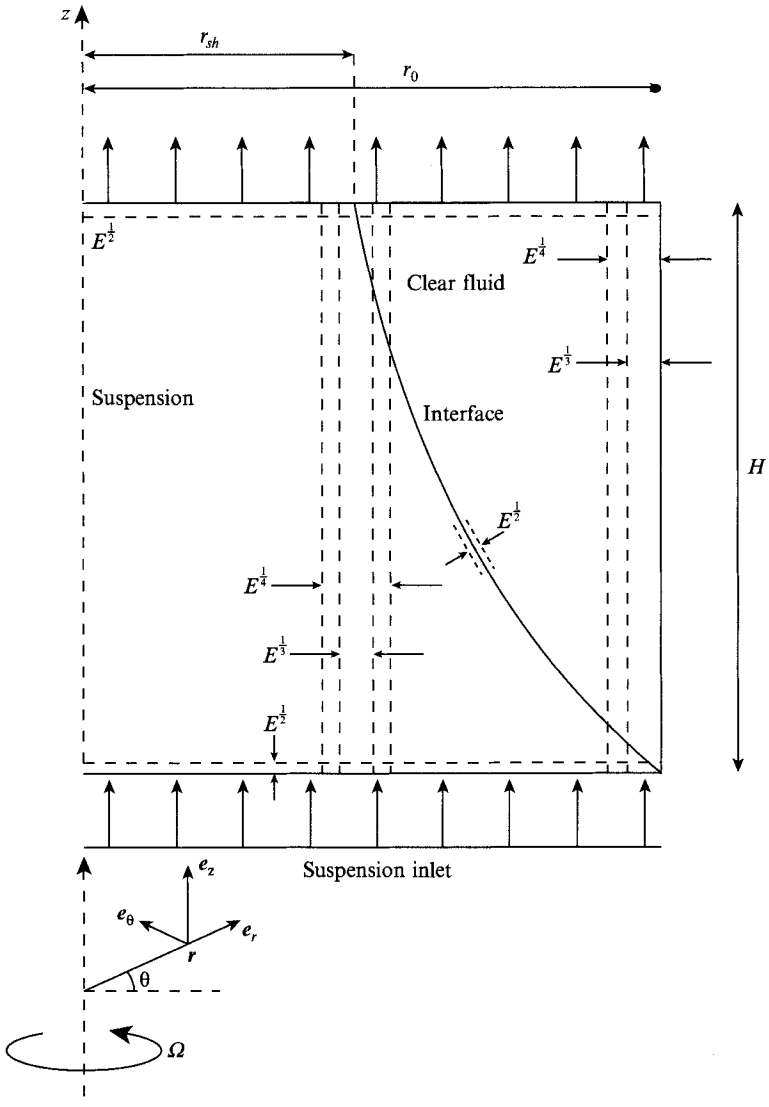

FIGURE 1. Sketch of geometry and of location and thickness of shear layers for small values of the Ekman number E.

and for the momentum balance of the mixture

$$(1+\epsilon\alpha)\,(Ro(\tfrac{1}{2}\nabla(\boldsymbol{q}\cdot\boldsymbol{q})+(\nabla\times\boldsymbol{q})\times\boldsymbol{q})+2\boldsymbol{e}_z\times\boldsymbol{q}) = -\nabla P+\frac{\epsilon\alpha}{Ro}\boldsymbol{r}$$

$$+E\nabla\cdot(\mu(\alpha)\,(\nabla\boldsymbol{q}+\nabla\boldsymbol{q}^{+}))-\frac{|\epsilon|^2\beta^2}{Ro}(1+\epsilon)\,\nabla\cdot\frac{\alpha(1-\alpha)}{1+\epsilon\alpha}\boldsymbol{q}_R\boldsymbol{q}_R, \quad (2.11)$$

where the Ekman number

$$E = \nu_C^*/\Omega^* r_0^{*2} \quad (2.12)$$

is based on the kinematic viscosity of the continuous phase, ν_C^*. The equations are

completed by a constitutive law for the relative velocity. An approximation appropriate for our purpose here is

$$\mu(\alpha)\boldsymbol{q}_R = -s(1-\alpha)\boldsymbol{e}_r[Ro^2(\tfrac{1}{2}\nabla(\boldsymbol{q}\cdot\boldsymbol{q})+(\nabla\times\boldsymbol{q})\times\boldsymbol{q})+Ro\,2\boldsymbol{e}_z\times\boldsymbol{q}+\boldsymbol{e}_z\times(\boldsymbol{e}_z\times\boldsymbol{e}_r r)]\cdot\boldsymbol{e}_r \tag{2.13}$$

where $s = |\epsilon|/\epsilon$. The right-hand side of (2.13) models the effective buoyant 'centrifugal force' on the particles as modified by inertial effects due to the motion of the mixture, and the left-hand side is the Stokesian drag force on the particles. Gravity is neglected because of the rapid rotation of the cylinder.

Since in most applications the particle Taylor number β is usually very small, the diffusion stresses due to the relative motion of the phases, represented by the last term in (2.11), are neglected in the analysis. Order-one effects of β on batch separation problems have been treated by e.g. Schaflinger *et al.* (1986) and Dahlkild & Greenspan (1989).

No-slip boundary conditions for the velocity field are assumed on the vertical as well as on the horizontal boundaries. The conditions at the top and bottom boundaries are thus similar to those of a porous wall with a specified velocity component normal to the boundary. Generally for an axisymmetric problem then

$$\boldsymbol{q}(r=1)=0, \tag{2.14}$$

$$\boldsymbol{e}_z\times\boldsymbol{q}(z=0)=\boldsymbol{e}_z\times\boldsymbol{q}(z=H)=0, \tag{2.15}$$

$$w(z=0)=w(z=H)=w_{in}(r), \tag{2.16}$$

where H is the non-dimensional height of the cylinder; $w_{in}(r)$ is the prescribed non-dimensional velocity distribution of the mixture injected at the inlet, identical to that of the fluid sucked out at the top. One may note here that (2.8), (2.13) imply $j_z = w$ even for non-zero particle volume fraction.

The particles entering the cylinder at the bottom were assumed to be well mixed in the fluid to a homogeneous suspension with volume fraction

$$\alpha(r, z=0)=\alpha_0, \tag{2.17}$$

whereas the concentration at the outlet followed from the solution. As no particles can penetrate the sidewall one must also require $\boldsymbol{j}_D\cdot\boldsymbol{e}_r = 0$ at $r = 1$. It follows then from (2.7), (2.14) and (2.13) that this is possible only if either $\alpha = 0$, i.e. there are no particles at the wall or the particles are at maximum packing $\alpha = \alpha_M$ for which $\boldsymbol{q}_R\cdot\boldsymbol{e}_r = 0$. The natural boundary condition for the volume fraction at the vertical sidewall is therefore

$$\alpha(r=1, 0<z\leqslant H)=\begin{cases}0, & s=-1\\ \alpha_M, & s=1,\end{cases} \tag{2.18}$$

since for particles heavier than the fluid settling towards the wall, a sediment layer will form, presumably at maximum packing for $r = 1$, and in the case of light particles settling inwards away from the sidewall, an outer region of clear fluid must appear adjacent to the wall.

As the mixture enters the cylinder the region of clarified fluid, or the sediment of settled particles formed, is separated from the mixture by a kinematic shock across which the particle concentration jumps discontinuously. Let the locus of this shock interface be given by

$$z=\Sigma(r) \tag{2.19}$$

and let the upward-pointing unit normal be

$$\boldsymbol{n} = \frac{\boldsymbol{e}_z - \Sigma'(r)\,\boldsymbol{e}_r}{(1+\Sigma'^2)^{\frac{1}{2}}}. \tag{2.20}$$

Then the stationary shock conditions at the interface are

$$[\boldsymbol{q}\times\boldsymbol{n}]^+_- = 0, \quad [\boldsymbol{j}\cdot\boldsymbol{n}]^+_- = 0, \quad [\boldsymbol{j}_D\cdot\boldsymbol{n}]^+_- = 0, \tag{2.21a–c}$$

$$Ro[(1+\epsilon\alpha)(\boldsymbol{q}\cdot\boldsymbol{n})^2]^+_- = -[P]^+_- + E[\boldsymbol{n}\cdot\boldsymbol{\Pi}\cdot\boldsymbol{n}]^+_-, \tag{2.21d}$$

$$Ro[(1+\epsilon\alpha)(\boldsymbol{q}\cdot\boldsymbol{n})\,\boldsymbol{n}\times\boldsymbol{q}]^+_- = E[\boldsymbol{n}\times\boldsymbol{\Pi}\cdot\boldsymbol{n}]^+_- \tag{2.21e}$$

where the stress tensor is

$$\boldsymbol{\Pi} = \mu(\alpha)(\nabla\boldsymbol{q} + \nabla\boldsymbol{q}^+).$$

These shock conditions express continuous velocity tangential to the surface, conservation of mixture volume, conservation of particles and conservation of mixture momentum in the normal and tangential directions respectively. Alternatively (2.21*b*) can be rewritten to express conservation of mixture mass

$$[(1+\epsilon\alpha)\,\boldsymbol{q}\cdot\boldsymbol{n}]^+_- = 0, \tag{2.21f}$$

where (2.21*c*), (2.7) and (2.8) have been used. The solution of the governing differential equations with boundary conditions thus include the determination of an interior boundary for which (2.21*a–e*) are provided and also serve as matching conditions for quantities on either side of the interface. To fix the position of the shock it was assumed that at $z = 0$ the interface was attached at $r = 1$ since the mixture was assumed well mixed at the inlet, i.e.

$$\Sigma(r=1) = 0. \tag{2.22}$$

This completes the general formulation of our problem. The analysis focuses on the case of light particles. For heavy particles a more sophisticated model for the sediment motion would probably be required for a realistic description of the flow in that region. It is known, for example, that particles in the sediment may resuspend owing to shear-induced migration. Experimental evidence as well as mathematical models of this phenomenon are at hand, see for example Leighton & Acrivos (1987*a*, *b*), Nir & Acrivos (1990) and Phillips, Armstrong & Brown (1992), but need to be explored further for simpler flow configurations before application to more complicated cases. The sediment motion, which really deserves a separate study, is thus left outside the scope of this paper.

3. Asymptotic analysis

The problem formulated in the previous section was studied in the limit of small Ekman number, $E \ll 1$. As discussed earlier β was also assumed small but considered to be of order one as $E \to 0$. The relative density difference ϵ was also assumed asymptotically small according to

$$|\epsilon| = cE^{\frac{1}{2}} \ll 1, \tag{3.1}$$

where $c = O(1)$. In addition to the axial throughflow the forcing mechanism of the flow during separation is buoyancy due to the density difference between the phases. A suitable Rossby number for the flow is therefore given by

$$Ro = |\epsilon| \ll 1 \tag{3.2}$$

which gives a balance in (2.11) between Coriolis and buoyancy forces if the particle volume fraction is considered $O(1)$. The magnitude of the vertical velocity, $Ro\, w_{in}\, \Omega^* r_0^*$, was chosen such that during the time a particle sedimented radially a distance $\sim r_0^*$ at a speed $\sim |\epsilon|\, \beta \Omega^* r_0^*$ it would be advected axially a distance $\sim H^*$. This was made clearer by defining

$$W = \frac{Row_{in}/H}{|\epsilon|\,\beta} = \frac{w_{in}}{\beta H} \sim 1, \tag{3.3}$$

which is used instead of w_{in} for the axial velocity at the inlet.

Formally the problem is solved by a perturbation procedure where a power series expansion in $E^{\frac{1}{2}}$ of the form

$$y(r, z) = y^0 + E^{\frac{1}{2}} y^1 + O(E) \tag{3.4}$$

is assumed for each of the dependent variables y. As is well known from the theory of rotating fluids, the inviscid limit $E \to 0$ is singular and the procedure must involve splitting the solution into asymptotically thin viscous boundary layers and larger regions of inviscid flow. Figure 1 shows the location of the various boundary layers that appeared in our case. At the horizontal boundaries Ekman layers of thickness $\sim E^{\frac{1}{2}}$ formed, by which the inviscid interior velocities were adjusted to the assumed no-slip condition at the wall. Ekman layers also appeared on each side of the kinematic shock which separated two different inviscid flow regions. Vertical shear layers of thicknesses $\sim E^{\frac{1}{3}}$ and $E^{\frac{1}{4}}$ formed not only on the sidewall but also at the radial position, r_{sh} say, where the kinematic shock reached the outlet at the top. These free shear layers were viscous transition layers which smoothed out the discontinuous angular velocity between the dynamically different inviscid flow regions on either side of $r = r_{sh}$. The Ekman layers were essential for the matching procedure with the inviscid regions whereas the vertical boundary layers were of passive nature and therefore not treated in detail.

In the subsequent sections we consider first, in §3.1, the inviscid interior flow from which also follows the basic stratification of the mixture. The matching to the Ekman boundary layers, required to completely determine the flow of the interior, is given special consideration in §3.2 with respect to the unconventional Ekman-layer structure due to the axial flow. Results for the complete interior flow are given in §4. Section 3.3 contains an analysis of the first-order effects on the concentration field due to secondary circulations in the interior. Results of the asymptotic analysis are compared with the numerical results in §5.

3.1. *The inviscid interior*

Neglecting viscous terms the governing equations (2.9)–(2.11) with (2.8) and (2.7) give to zeroth order in $E^{\frac{1}{2}}$

$$\nabla \cdot \boldsymbol{q}^0 = 0, \tag{3.5}$$

$$\boldsymbol{q}^0 \cdot \nabla \alpha^0 = -\beta \nabla \cdot (\alpha^0 (1 - \alpha^0)\, \boldsymbol{q}_R^0), \tag{3.6}$$

$$2\boldsymbol{e}_z \times \boldsymbol{q}^0 = -\nabla P^0 + s\alpha^0 r \boldsymbol{e}_r, \tag{3.7}$$

where $s = -1$ for light particles. For the relative velocity, (2.13) to zeroth order yields

$$\boldsymbol{q}_R^0 = s \frac{1 - \alpha^0}{\mu(\alpha^0)} r \boldsymbol{e}_r. \tag{3.8}$$

Since there is no change in the axial velocity in the Ekman layers to lowest order the appropriate boundary conditions for the inviscid flow outside the boundary layers at the in- and outlet are

$$w^0(z=0) = w^0(z=H) = w_{in}(r) = \beta HW(r). \tag{3.9a, b}$$

The solution of (3.5) and (3.7) with (3.9) gives

$$u^0 = 0, \tag{3.10}$$

$$v^0 = \frac{1}{2}\frac{\partial}{\partial r}P^0 - s\alpha^0\frac{r}{2}, \tag{3.11}$$

$$\frac{\partial}{\partial z}P^0 = 0, \tag{3.12}$$

$$w^0 = \beta HW(r), \tag{3.13}$$

where (3.12) implies

$$\frac{\partial}{\partial r}P^0 = G(r). \tag{3.14}$$

To obtain the degrees of freedom necessary for the inviscid solution to adjust to the shock conditions, the arbitrary function $G(r)$ for $r > r_{sh}$ formally had to be split into two parts, G^+ and G^- say, representing respectively integrations of (3.12) above and below the clear fluid–suspension interface. However, it follows from the shock condition (2.21*d*) to zeroth order that the pressure is continuous across the interface, whereby $G^+ = G^-$. Note here that the interface is embedded within two Ekman layers which really requires the shock conditions to be evaluated with the boundary-layer solution at the shock. The procedure above could be justified though, as the boundary-layer correction to the pressure in Ekman layers did not change to lowest order. Since the boundary-layer correction of the normal velocity component was also zero to lowest order, the same procedure could be applied for (2.21*f*) to zeroth order to confirm that the inviscid solution above conserved the mixture mass flow normal to the shock. The properties of the Ekman layers stated above are derived in Appendix A.

Without further knowledge of the pressure gradient and the azimuthal velocity component the analysis continued with the determination of the concentration field $\alpha^0(r, z)$, which also involved the determination of $\Sigma(r)$, the vertical position of the clear fluid–suspension interface. For convenience the conservation equation for the particles to zeroth order (3.6) with (3.8) is written in characteristic form

$$\frac{\mathrm{d}}{\mathrm{d}z}\alpha^0 = -\frac{2s\beta}{w^0}\frac{\alpha^0(1-\alpha^0)^2}{\mu(\alpha^0)}, \tag{3.15a}$$

$$\frac{\mathrm{d}}{\mathrm{d}z}r^0 = \frac{s\beta r^0}{w^0}\frac{d}{d\alpha}\left\{\frac{\alpha(1-\alpha)^2}{\mu(\alpha)}\right\}\Bigg|_{\alpha=\alpha_0}, \tag{3.15b}$$

where $r^0(z)$ is the characteristic path to zeroth order. A solution to (3.15) of the following form was found

$$\frac{r^0}{r_i^0} = \left(\frac{\alpha_i^0(1-\alpha_i^0)^2/\mu(\alpha_i^0)}{\alpha^0(1-\alpha^0)^2/\mu(\alpha^0)}\right)^{\frac{1}{2}}, \tag{3.16a}$$

$$\frac{z^0 - z_i^0}{H} = -\int_{\alpha_i^0}^{\alpha^0} W(r^0(\alpha))\frac{\mu(\alpha)}{2s\alpha(1-\alpha)^2}\,\mathrm{d}\alpha, \tag{3.16b}$$

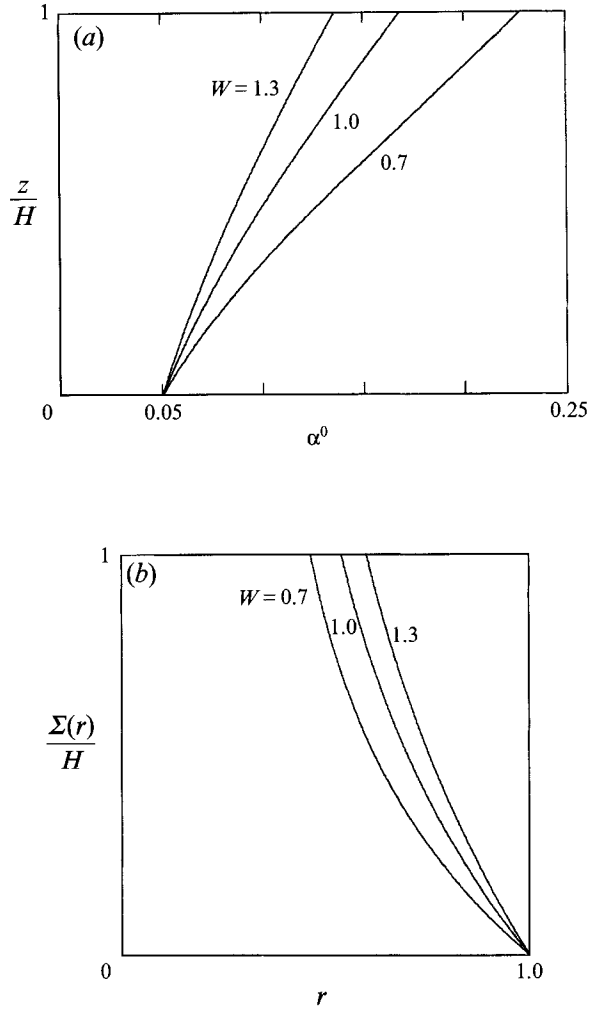

FIGURE 2. (*a*) Volume fraction of light particles versus the axial coordinate and (*b*) the shape of the clear fluid–suspension interface in the case of uniform axial flow for $\alpha_0 = 0.05$, $W = 0.7$, 1.0, 1.3.

where α^0 is used as a parameter to obtain the characteristic path (r^0, z^0). The starting point of the characteristics is at the inlet $z_i^0 = 0, 0 \leqslant r_i^0 \leqslant 1$ where, by (2.17), $\alpha_i^0 = \alpha_0$. Characteristics also originate at $r_i^0 = 1, 0 \leqslant z_i^0 \leqslant H$, for which it is sufficient to know that they cross the characteristics originating at the inlet and thus yield the value $\alpha = 0$ for light particles on the upper side of the kinematic shock. It might be of some interest to mention that there are some similarities in the result (3.16) and the work by Ungarish (1991) on the spin-up of a suspension.

For the case of a uniform axial velocity, so that W is independent of r, the volume fraction is also independent of the radial coordinate and obtained directly from (3.16*b*). Figure 2(*a*) shows the concentration for light particles for $\alpha_0 = 0.05$ and different values of W. For light particles, then, the concentration gradient is in the positive axial direction and increasing for smaller axial velocities owing to the increased time spent by a mixture fluid element in the cylinder. Following a mixture fluid element from the inlet and through the cylinder in the case of uniform axial flow, the time-

dependent variation of the particle volume fraction would be completely analogous to that of centrifugal batch settling of a homogeneous suspension. The approximation for dilute suspensions obtained from (3.16*b*) is

$$\alpha^0(z) = \alpha_0 \mathrm{e}^{-2s\frac{z/H}{W}}, \tag{3.17}$$

which is also similar in form to the time-dependent case.

The continuous stratification of the mixture extended up to the position of the kinematic shock for which (2.21*c*) yields

$$[\alpha^0 \boldsymbol{q}^0 \cdot \boldsymbol{n}^0]_-^+ + s\beta \left[\frac{\alpha^0(1-\alpha^0)^2}{\mu(\alpha^0)}\right]_-^+ r\boldsymbol{e}_r \cdot \boldsymbol{n}^0 = 0 \tag{3.18}$$

to zeroth order. The velocity field in the first term can be evaluated with the zeroth-order inviscid solution only since the Ekman-layer correction at the shock of the normal velocity component is zero to this order (see Appendix A). For light particles $\alpha^+ = 0$ and (3.18) with (3.10), (3.11) and (2.20) gives

$$HW(r) + \frac{(1-\alpha^-(r))^2}{\mu(\alpha^-(r))} \Sigma'(r)\, r = 0, \tag{3.19}$$

with zeroth-order superscripts omitted. The straightforward interpretation of (3.19) is that the interface is obtained by tracing a sedimenting particle convected in the axial velocity field from the outer rim of the inlet to the outlet. In the dilute limit $\alpha^- = 0$ an integral of (3.19) is easily obtained. For non-dilute suspensions, though, (3.19) must be combined with the solution for the volume fraction (3.16) evaluated at the shock

$$\Sigma(r) = H \int_{\alpha_0}^{\alpha^-(r)} W\left\{r\left[\frac{\alpha^-(r)\,(1-\alpha^-(r))^2/\mu(\alpha^-(r))}{\alpha(1-\alpha)^2/\mu(\alpha)}\right]^{\frac{1}{2}}\right\} \frac{\mu(\alpha)}{2\alpha(1-\alpha)^2}\,\mathrm{d}\alpha. \tag{3.20}$$

The complicated argument in W is the local radial position of the characteristic path during the integration from the inlet to the position of the shock. Equation (3.19) with (2.22) and (3.20) are sufficient to determine $\Sigma(r)$ and $\alpha^-(r)$ to zeroth order in $E^{\frac{1}{2}}$ for any axial velocity profile $W(r)$.

The solution procedure is greatly simplified in the case of a uniform axial flow for which an explicit integral of the particle volume fraction at the interface can be obtained:

$$\alpha^-(r) = \alpha_0 / r^2. \tag{3.21}$$

The axial position of the interface $\Sigma(r)$ is then given by (3.20), for which the dilute limit approximation can be derived from (3.17) with $\alpha^0 = \alpha^-(r)$ and $z = \Sigma(r)$ as

$$\Sigma(r) = HW \ln(1/r). \tag{3.22}$$

The interface shape obtained in the non-dilute case is shown in figure 2(*b*) for the same parameter settings as in figure 2(*a*). As expected, the clear fluid region was larger for smaller axial velocities. The curved shape of the interface was caused mainly by the decreased settling velocity at smaller radii but also by the increased hindering effect at larger particle concentrations.

In the preceding analysis the determination of the concentration field and the position of the clear fluid–suspension interface to the first approximation are obtained without knowledge of the complete velocity field. Only the inviscid axial flow is needed

which extends unchanged through the cylinder. The azimuthal motion on the other hand is an effect of the continuous stratification of the mixture and the sudden density change across the shock. Differentiation of (3.11) yields

$$\frac{\partial}{\partial z}v^0 = -s\frac{r}{2}\frac{\partial}{\partial z}\alpha^0 = -\frac{1}{2Ro}[\nabla(1+\epsilon\alpha)\times\nabla(\tfrac{1}{2}r^2)]\cdot\boldsymbol{e}_\theta, \tag{3.23}$$

which is analogous to the 'thermal wind equation' for a baroclinic atmosphere (see e.g. Pedlosky 1987, p. 42). The continuous stratification thus induces a vertical gradient of the azimuthal flow. Similarly the density jump at the clear fluid-suspension interface results in a discontinuous variation of the inviscid azimuthal velocity across the interface:

$$[v^0]_-^+ = s\tfrac{1}{2}r\alpha^0(\Sigma(r)). \tag{3.24}$$

To complete the determination of the azimuthal velocity, the inviscid problem must be considered to next order in $E^{\frac{1}{2}}$. An equation for the reduced pressure gradient $G(r)$ then results from the compatibility conditions of the secondary inviscid flow with the various Ekman layers.

To first order in $E^{\frac{1}{2}}$ the inviscid azimuthal component of (2.11) with (3.13) is

$$c\beta H\, W(r)\frac{\partial}{\partial z}v^0 + 2u^1 = 0 \tag{3.25}$$

which with (3.23) yields

$$u^1 = sc\beta HW(r)\tfrac{1}{4}r\frac{\partial}{\partial z}\alpha^0. \tag{3.26}$$

It is thus found that the mass-averaged radial velocity component of the inviscid interior flow is negative which is rather surprising since during separation one would expect an outward radial massflow which is the direction of the centrifugal force. However, this result is caused instead by the conservation of total angular momentum of a mixture fluid element followed through the container. For, the increasing azimuthal velocity according to (3.23) corresponds to an increasing angular momentum which thus must be compensated for by a small inward displacement of the mixture fluid element to maintain the same total angular momentum. This is quantified for the phase-averaged radial velocity by (3.26).

In terms of mass-averaged velocity components the mixture continuity equation (2.9) to first order with (3.26) gives

$$\frac{\partial}{\partial z}w^1 + \frac{1}{r}\frac{\partial}{\partial r}\left(sc\beta HW(r)\frac{r^2}{4}\frac{\partial}{\partial z}\alpha^0\right) = sc\beta\nabla\cdot(\alpha^0(1-\alpha^0)\boldsymbol{q}_R^0). \tag{3.27}$$

The source term in the mass conservation equation (3.27) shows that a mass element of the mixture expands owing to the separation of the phases. As the radial mass flow obtained in (3.26) typically corresponds to a contraction of the fluid in the radial direction, the whole flow divergence is manifested as a vertical stretching of fluid elements. The corresponding axial velocity thus directs the mass flow towards the boundaries where it is redirected outwards by the divergent Ekman layer flow. Using (3.6), (3.27) can be integrated to obtain the vertical component of the secondary flow

$$w^1(r,z) = -s\frac{W(r)}{\lambda}\alpha^0(r,z) - s\frac{1}{r}\frac{\partial}{\partial r}\left(\frac{W(r)}{\lambda}\frac{r^2}{4}\alpha^0(r,z)\right) + D(r). \tag{3.28}$$

Here the arbitrary function $D(r)$, obtained from the integration, is, similar to $G(r)$, split into D^+ and D^- for $r > r_{sh}$. The new parameter λ introduced in (3.28),

$$\lambda \equiv \frac{1}{c\beta H} = \frac{E^{\frac{1}{2}}}{|\epsilon|\beta H}, \tag{3.29}$$

is for batch settling problems, as in Ungarish (1986), and is usually interpreted as the ratio of the separation time to the spin-up time in the cylinder which might be somewhat confusing here since the process is stationary. A more appropriate interpretation would be the relative strength, per unit length in the azimuthal direction, of the typical Ekman layer mass flux, $Ro\,\Omega^* r_0^* E^{\frac{1}{2}} r_0^*$, and the phase-averaged radial mass flux induced by the separation, $|\epsilon|^2 \beta \Omega^* r_0^* H^*$, as estimated from (2.8). (This interpretation should apply also to more generally formulated stationary separation processes than the one studied here.)

For the case of a uniform inlet profile we may summarize the inviscid solution for the azimuthal velocity as

$$v^0(r,z) = \tfrac{1}{2}(G(r) - s\alpha^0(z)\, r) \tag{3.30}$$

and the meridional velocity components including the secondary flow may be simplified to

$$w(r,z) = \beta H W(1 - \epsilon\tfrac{3}{2}\alpha^0(z)) + E^{\frac{1}{2}} D(r), \tag{3.31a}$$

$$u(r,z) = -|\epsilon|\,\beta \frac{r}{2} \frac{\alpha^0(z)\,(1-\alpha^0(z))^2}{\mu(\alpha^0(z))}. \tag{3.31b}$$

$D(r)$ was determined together with $G(r)$ from the equivalent boundary conditions of the inviscid flow obtained from the analysis of the Ekman layers.

3.2. *Matching to the Ekman layers with suction or injection*

The Ekman layers are not of standard type as they appear within an axial flow of the same order of magnitude as the flow in the Ekman layer itself. Ekman-layer pumping velocities, necessary for the matching procedure to the interior, in the case of rigid-body rotation outside the Ekman layers might be obtained from limiting values far away from the disk of the similarity solution of Rogers & Lance (1960). However, such a procedure would be quite inconvenient and much too complex in our case, nor was it necessary to serve our purposes in the parameter regimes considered. We consider for that reason the modified linear Ekman-layer flow at a surface, $z = Z(r)$, with upward pointing normal, $\boldsymbol{l}$, say, with either suction or injection. The Ekman layers above $z = 0$ and on the upper side of the kinematic shock are thus of the injection type whereas the Ekman layers below $z = H$ and on the lower side of the shock are of the suction type. The analysis of these flows is only briefly outlined here. The details are given in Appendix A.

It was found that the axial velocity as well as the particle volume fraction are unchanged to zeroth order through the boundary layer. A linear boundary layer equation was then derived that included a term representing axial convection of momentum through the Ekman layer. The strength of this effect was measured by the ratio of the injection velocity and the Ekman-layer viscous diffusion velocity

$$\Gamma \equiv \frac{w_{in}^*}{(\Omega^* \nu_0^*)^{\frac{1}{2}}} = \frac{W(r)}{\lambda}. \tag{3.32}$$

As this was assumed to be an order-one quantity, considerable modifications of the Ekman-layer flow appeared for non-zero values of this ratio. Figure 3(*a*) shows a

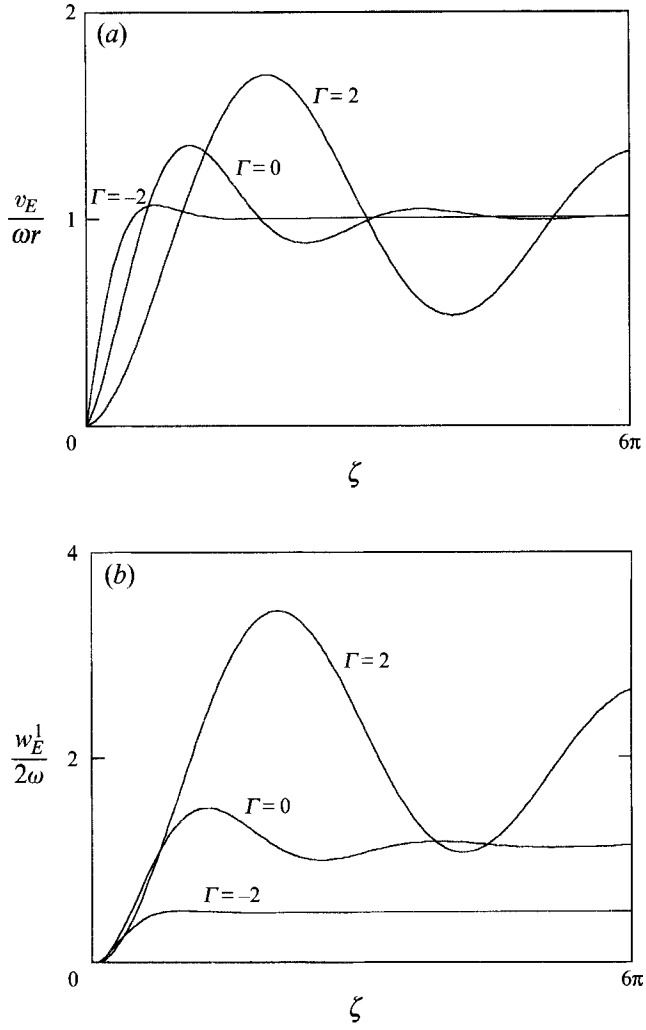

FIGURE 3. Divergent Ekman-layer flow at a horizontal boundary with suction or injection for rigid-body-rotation inviscid flow, ωr, as $\zeta \to \infty$; $\Gamma = 0, \pm 2.0$. (*a*) Azimuthal velocity component. (*b*) Secondary vertical velocity component.

graph of the normalized azimuthal velocity component versus the boundary-layer coordinate ζ for different values of Γ at a horizontal boundary. Positive and negative signs on Γ are used to indicate respectively injection and suction of fluid at the boundary. For $\Gamma = 0$ the ordinary Ekman-layer solution was retained with boundary-layer thickness $\delta_E \sim E^{\frac{1}{2}}(\mu_Z/\boldsymbol{l}\cdot\boldsymbol{e}_z)^{\frac{1}{2}}$, but for $\Gamma > 0$ the Ekman layer was wider and with pronounced oscillations. For $\Gamma < 0$ it appeared thinner and with suppressed oscillations. For large values of $|\Gamma|$ the boundary-layer thicknesses of the injection and the suction layers were respectively $\delta_E \sim E^{\frac{1}{2}}\Gamma$ and $\delta_E \sim E^{\frac{1}{2}}\mu_Z/(\Gamma\boldsymbol{l}\cdot\boldsymbol{e}_z)$. The normal velocity component obtained, which was needed for the matching procedure to the secondary inviscid flow, is shown in figure 3(*b*). The value approached for large values of the boundary-layer coordinate, which is also a measure of the mass flow in the Ekman layer, increased/decreased for a pronounced injection/suction rate.

The derivation of the compatibility conditions for the secondary inviscid flow that appear from the matching procedure to the boundary-layer flow is given in Appendix

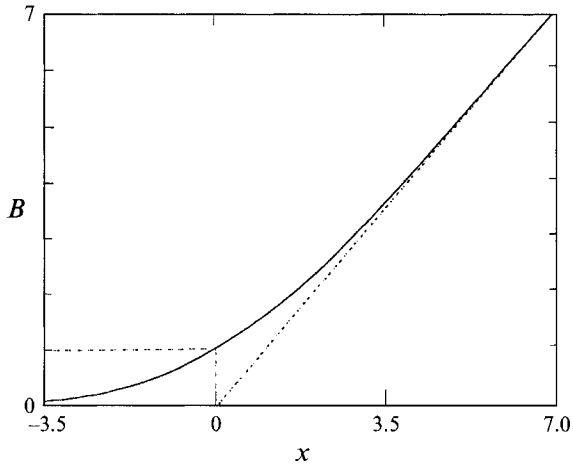

FIGURE 4. The relative strength, $B[\gamma(x; \boldsymbol{e}_z)]$, of the Ekman-layer pumping in a divergent Ekman layer with suction or injection versus injection rate x.

B. The boundary-layer analysis is valid for arbitrary axial velocity profiles but the matching was performed in detail only for the case of a uniform inlet profile.

At the horizontal boundaries the boundary conditions obtained for the secondary vertical velocity component are

$$w^1(z=0) = \tfrac{1}{2}[\mu(\alpha_0)]^{\frac{1}{2}} \frac{1}{r}\frac{\partial}{\partial r}(rv^0(z=0))\, B\left[\gamma\left(\frac{\Gamma}{\mu_0^{\frac{1}{2}}}; \boldsymbol{e}_z\right)\right], \tag{3.33}$$

$$w^1(z=H) = -\tfrac{1}{2}[\mu(\alpha_H^0)]^{\frac{1}{2}} \frac{1}{r}\frac{\partial}{\partial r}(rv^0(z=H))\, B\left[\gamma\left(\frac{-\Gamma}{\mu_H^{\frac{1}{2}}}; \boldsymbol{e}_z\right)\right], \tag{3.34}$$

where subscripts 0 and H denote evaluation at $z=0$ and $z=H$ respectively. The definition of B is

$$B[\gamma] = 2\frac{Re\{\mathrm{i}\gamma\}}{|\gamma|^2} \tag{3.35}$$

and the complex function γ is defined by (A 9) of Appendix A. A graph of $B[\gamma(x; \boldsymbol{e}_z)]$ versus x is shown in figure 4 which thus, according to (3.33) and (3.34), gives the relative change of the Ekman-layer suction for a given flow divergence of the outer flow. It is also a measure of the relative mass transport efficiency of the Ekman layer. For $x=0$, corresponding to the limit $\Gamma=0$, we have $\gamma = 1-\mathrm{i}$ and thus $B[\gamma]=1$ so that (3.33) and (3.34) reduce to the ordinary Ekman-layer compatibility relations. With suction at the boundary, corresponding to a negative value of x in figure 4, B and the secondary inviscid flow were smaller in magnitude and approached zero for strong suction. A reinforced secondary flow was obtained with injection at the boundary where B approached the line $B=x$ for large values of x.

In the region $r > r_{sh} = (\alpha_0/\alpha_H^0)^{\frac{1}{2}}$ the inviscid solution must also be compatible with the Ekman layers at the clear fluid–suspension interface. The first-order expansion of (2.21f) together with the Ekman-layer solution implies that for the vertical velocity component of the secondary inviscid flow

$$[w^1]_-^+ = -s\frac{3W}{2\lambda}[\alpha^0]_-^+ + \frac{W}{2\lambda}\left[\frac{1}{r}\frac{\partial}{\partial r}(rv^0) + \Sigma'(r)\frac{\partial}{\partial z}v^0\right]_-^+. \tag{3.36}$$

The boundary conditions (3.33), (3.34) and (3.36) can now be used with the inviscid solution to determine the functions $G(r)$ and $D(r)$. However, as the conditions above yield a differential equation for $G(r)$, an additional requirement has to be imposed on the flow. This is obtained from the global conservation of volume in the cylinder. Since the axial in- and outlet profiles are identical the volume flow across any cylindrical surface centred around the rotation axis must equal zero, i.e.

$$J_r = 2\pi r \int_0^H \boldsymbol{j}\cdot\boldsymbol{e}_r \,\mathrm{d}z = 0. \tag{3.37}$$

Explicit use of (3.37) and the resulting expressions for $G(r)$ and $D(r)$ are presented in Appendix C.

Although the global radial volume flux is zero this does not hold for the corresponding mass flow since separation of the phases takes place. The global radial mass flow, Q_r, can be obtained by observing (see Appendix C) that the interior mass flux is one third of the volume flux and that the Ekman layer mass and volume fluxes are the same to lowest order. Thus, with J_E and J_I representing order-one quantities of the Ekman layer and interior volume fluxes and since $J_E = -J_I$

$$Q_r = E^{\frac{1}{2}}(J_E + \tfrac{1}{3}J_I) = -E^{\frac{1}{2}}\tfrac{2}{3}J_I = \begin{cases} |\epsilon|\,\beta H W \pi r^2 \alpha_0 \left[\dfrac{1}{r_{sh}^2} - 1\right] & \text{for} \quad r \leqslant r_{sh} \\ |\epsilon|\,\beta H W \pi r^2 \alpha_0 \left[\dfrac{1}{r^2} - 1\right] & \text{for} \quad r \geqslant r_{sh} \end{cases}, \tag{3.38}$$

where (3.21) has been used to eliminate α^- and α_H^0 in the formula for J_I in Appendix C.

3.3. *First-order analysis of the density stratification*

With the flow field established, first-order corrections to the concentration field were considered mainly in order to verify the results from the numerical analysis. Corrections to the stratification that we considered originated in two different physical effects. First, the azimuthal motion of the mixture changes the effective centrifugal force on the particles; of the higher-order terms in the constitutive law for the relative velocity, (2.13), the Coriolis acceleration of the mixture is retained in the conservation equation for the particles. Thus, the rate at which separation occurs for the axially convected fluid elements changes. Secondly the secondary circulation of the mixture changes the axial convective transport of the particles which also affects the stratification.

In characteristic form the conservation equation for the particles, including the first-order corrections, is

$$\frac{\mathrm{d}}{\mathrm{d}z}\alpha = -\frac{2s\beta}{w^0 + E^{\frac{1}{2}}w^1}\frac{\alpha(1-\alpha)^2}{\mu(\alpha)}\left[1 + |\epsilon|\frac{1}{r}\frac{\partial}{\partial r}(rv^0)\right], \tag{3.39a}$$

$$\frac{\mathrm{d}}{\mathrm{d}z}r = \frac{s\beta r}{w^0 + E^{\frac{1}{2}}w^1}\frac{\mathrm{d}}{\mathrm{d}\alpha}\left\{\frac{\alpha(1-\alpha)^2}{\mu(\alpha)}\right\} + E^{\frac{1}{2}}3u^1. \tag{3.39b}$$

To obtain a solution correct to first order in $E^{\frac{1}{2}}$ it is sufficient to evaluate the solution of (3.39*a*) on the zeroth-order expansion of the characteristic paths. Since the concentration to zeroth order, $\alpha^0(z)$, is independent of r in the suspension region, a first-order correction to the characteristic paths would, except for a small correction of the shock position, give only second-order corrections to the concentration. The

procedure is simplified by the fact that separately in the regions $r < r_{sh}$ and $r > r_{sh}$ the vorticity of the azimuthal flow and the first-order vertical velocity are functions only of z. Subsequently the separate solutions obtained in the regions inside and outside $r = r_{sh}$ are also functions only of z except for a radial region corresponding to those characteristics that appeared on both sides of $r = r_{sh}$. The latter region continuously connects the two former, differently stratified, regions.

One should note here that the flow within the free vertical shear layers at $r = r_{sh}$ is not considered here. Consideration of flow within these layers would give additional corrections to the concentration field of order $E^{\frac{1}{2}}$ in the interconnecting region mentioned above. However, the complicated study of these layers to obtain a formally correct solution there is far beyond the purpose of this study.

The position of the interface was also corrected to first order but the analysis is omitted here. Results of the analysis obtained from this section have been compared with the numerical solution (see figures 8 and 10).

4. Asymptotic results

The asymptotic results for the case of uniform axial flow for $W = 0.7$ are presented next. The inlet concentration was $\alpha_0 = 0.05$ which gave $\alpha^0(z = H) = 0.23$ and thus $r_{sh} = 0.47$.

In the region $r < r_{sh}$ the azimuthal velocity component is linear in the radial coordinate and the axial variation for $\Gamma = W/\lambda = 0.2, 2.0$ is shown in figure 5. Away from the Ekman layers the velocity distribution directly maps the density stratification according to (3.11). As the stratification is independent of Γ, changing the value of this parameter just results in a displacement of the profile towards more negative values with the interior shape intact. This shift of the velocity is required by the changed radial volume flux balance of the interior and the Ekman layers. For $\Gamma = 0$ (or equivalently $1/\lambda = 0$) the interior radial flow is negligible compared to the Ekman layer flow, so that the Ekman fluxes are of equal magnitudes but in opposite directions, outwards at the inlet and inwards at the outlet. For non-zero Γ the secondary inward interior flux, $\sim E^{\frac{1}{2}}W/\lambda = E^{\frac{1}{2}}\Gamma$, must be compensated for by a net outward flow in the Ekman layers; the negative shift of the velocity at $z = 0$ thus reinforces the outward flow there whereas at $z = H$ the flux is suppressed or even changes direction. For large values of Γ the suction effect on the Ekman layer at $z = H$ completely blocks the flow in this layer. The outward flow is therefore concentrated in the Ekman layer at $z = 0$ where the changed boundary-layer structure due to axial injection allows increased radial mass transport. The magnitude of the azimuthal velocity therefore increases in a range of moderate Γ, whereas for larger values of Γ the increased mass transport in the Ekman layer is sustained by a larger relative transport efficiency with the azimuthal velocity approximately unchanged.

The axial variation of the azimuthal velocity at $r = 0.66 > r_{sh}$ is shown in figure 6. Above the shock in the homogeneous clear fluid the velocity is constant in contrast to the flow in the stratified mixture region. Owing to the large density increase across the interface, the resulting difference between the azimuthal edge velocities of the Ekman layers at the outlet and inlet is negative for $r > r_{sh}$. For the case $\Gamma = 0$ or small, this requires the Ekman fluxes at the boundaries to be inwards at the inlet and outwards at the outlet which are in opposite directions compared to the fluxes in the region inside the vertical shear layers. For non-zero values of Γ and radial positions $r > r_{sh}$ the volume flux balance is more complex as it also involves non-divergent contributions. The azimuthal velocity thus includes an irrotational part to allow such transports in the

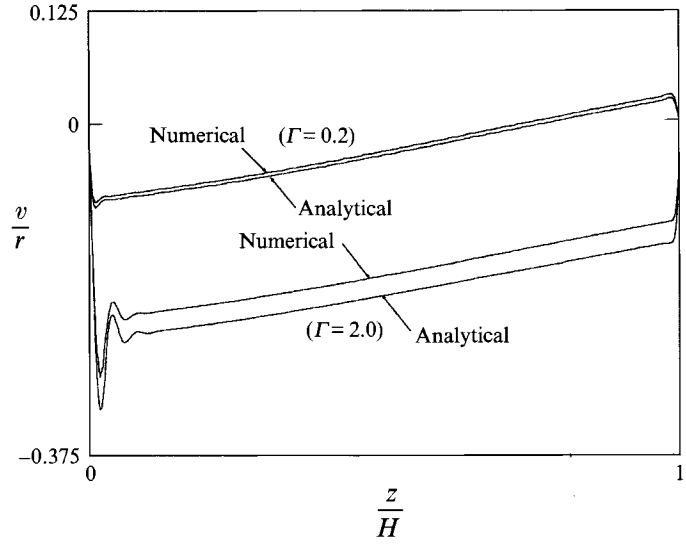

FIGURE 5. Azimuthal velocity profile versus the axial coordinate at $r = 0.15 < r_{sh}$ for $\Gamma = 0.2$ and 2.0. Comparison of the analytical and numerical solutions. $W = 0.7$, $E = 0.25 \times 10^{-4}$, $\alpha_0 = 0.05$, $\beta = 0.05$.

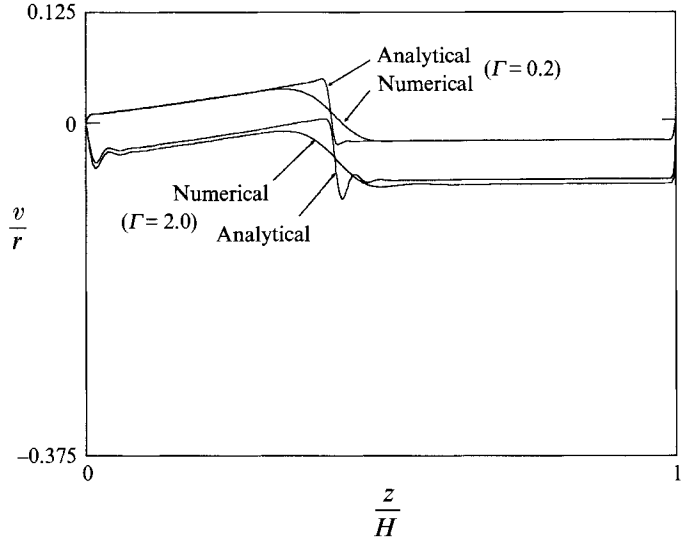

FIGURE 6. Azimuthal velocity profile versus the axial coordinate at $r = 0.66 > r_{sh}$ for the same cases as in figure 5. Comparison of the analytical and numerical solutions.

Ekman layers. Therefore, the shift of v/r with Γ varies with the radial position but shows the same type of behaviour as that discussed for $r < r_{sh}$.

The secondary flow in the (r, z)-plane is responsible for the interior radial flow and the redistribution into the Ekman layers. Figure 7 shows a schematic of the Ekman layer fluxes, J_E, and the interior secondary flow for the typical cases of $\Gamma \ll 1$ and $\Gamma \gtrsim 1$. Also indicated in figure 7 are the directions of the axial secondary velocity, w^1, and of the vertical boundary layer fluxes, J_V, which are necessary to close the secondary flow in the meridional plane. For small values of Γ the interior radial flow is negligible compared to the Ekman layer fluxes and is therefore not shown at all in

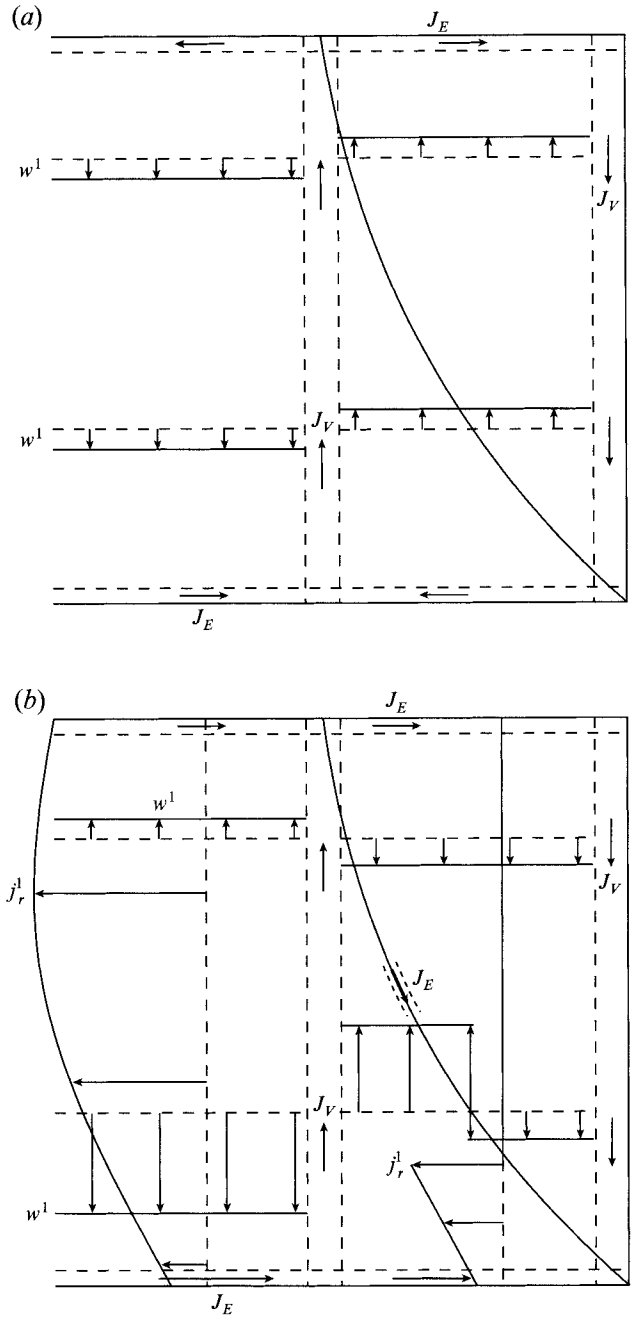

FIGURE 7. Qualitative picture of secondary flow in a meridional plane for (*a*) $\Gamma \ll 1$ and (*b*) $\Gamma \gtrsim 1$.

figure 7(*a*). Figure 7(*b*) shows the phase-averaged radial volume flux velocity versus the axial coordinate at two different radial positions: $r < r_{sh}$ and $r > r_{sh}$. The increased magnitude with the axial coordinate reflects the response of the radial flow to the intensified swirl flow gradient. Although the radial 'mixture' velocity is negative the velocity of the heavy clear fluid phase is positive and an order of magnitude larger, as calculated from (3.8) and the definitions of the averaged velocities and of the relative velocity.

The axial secondary velocity versus z for $r < r_{sh}$ is discussed next. When the interior radial flow is negligible compared to the Ekman layer flow, $\Gamma \equiv W/\lambda = 0$, the secondary vertical velocity is independent of z, just communicating the opposite divergent Ekman-layer flows at the top and bottom. At larger values of Γ, the axial stretching of fluid elements required to redirect the convergent radial volume flow towards the Ekman layers accumulates as a vertical velocity difference between the top and bottom. For large values of Γ the flow is only into the lower Ekman layer as suction blocking of the top Ekman layer diminishes this velocity. At radial positions $r > r_{sh}$ the decreasing area of the radially projected mixture region changes the vertically integrated interior radial volume flow which is here divergent rather than convergent. The net vertical flow for $\Gamma \gtrsim 1$ is therefore out from the Ekman layers in this region as sketched in figure 7(*b*). Across the interface the jump of the inviscid vertical velocity component is required by mass conservation between the interior flows only since the Ekman layers there are non-divergent.

5. Numerical simulation

The numerical analysis used a slightly extended version of a code for solving the 'mixture model' equations presented recently in a paper by Amberg & Ungarish (1993). They study the spin-up of a mixture from rest in a cylinder, which is a strongly nonlinear problem. In their case the small divergence of the mass-averaged velocity due to separation is neglected which can be justified since there the Rossby number is of order one and the secondary flow due to Ekman-layer circulation is an order of magnitude larger than the flow induced by separation.

For the case studied in the present paper, the Rossby number is small and the flow is driven instead by the separation process itself. As the global mass transport due to separation is of the same order of magnitude as the induced secondary flow in the parameter regime considered, the mass flow divergence had to be retained in the code; explicitly

$$\nabla \cdot \boldsymbol{q} = \epsilon \frac{|\epsilon| \beta}{Ro} \nabla \cdot \left(\frac{\alpha(1-\alpha)}{(1+\epsilon\alpha)} \boldsymbol{q}_R \right). \tag{5.1}$$

Further details on the code, which uses a time-stepping procedure of a pressure correction scheme originally by van Kan (1986), are given by Amberg & Ungarish (1993).

The program was started with the whole cylinder filled with a homogeneous mixture and was run through a smooth transient until a steady state was reached. Otherwise, the formulation for the numerical analysis followed mainly that in the second section of this paper, including the identical in- and outflow conditions for the velocity. The treatment of the clear fluid–suspension interface was different though. The shock was here captured by the code rather than fitted to the shock conditions (2.21*a–e*). A smooth variation of the concentration at the position of the interface thus resulted from artificially introduced diffusion terms in the conservation equation of the particles. The Ekman layers at the interface were therefore poorly reproduced. An important question to resolve was if this would have a large effect on the flow field in general owing to the interaction between the interior and the Ekman layers. The number of grid points used were in both cases 60 in the radial and 200 in the axial direction which appeared to be sufficient for numerical resolution of the various boundary layers at the present parameter settings.

Two cases with different values of Γ were analysed and compared with the results of the asymptotic analysis. Identical parameter values in the two cases were the Ekman

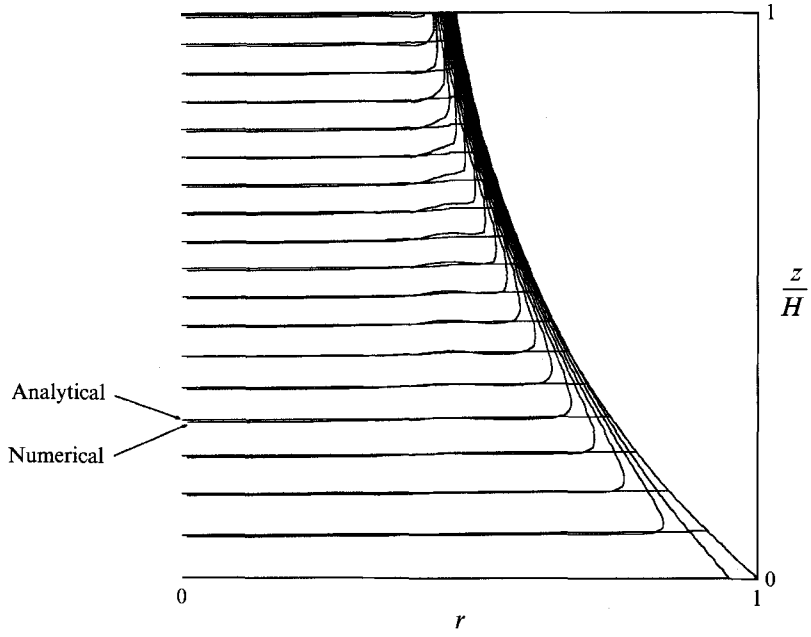

FIGURE 8. Comparison between analytical and numerical solution of iso-concentration lines in a meridional plane; $\Gamma = 0.2$, $E = 0.25 \times 10^{-4}$, $W = 0.7$, $\alpha_0 = 0.05$, $\beta = 0.05$. $\alpha = 0.05 + i \times 0.01$, $i = 0, 1, \ldots, 17$.

number, $E = 0.25 \times 10^{-4}$, the particle Taylor number, $\beta = 0.05$, the non-dimensional injection velocity, $w_{in} = 0.035$, the aspect ratio, $H = 1$ and the inlet concentration, $\alpha_0 = 0.05$. Equivalently $W = w_{in}/\beta H = 0.7$ which means that the interface and the concentration field will be approximately the same in both cases considering the result of the analytical solution. The two cases were distinguished by $\Gamma = W/\lambda = 0.2$ and $\Gamma = 2.0$. For the values of the six independent parameters $E, \beta, H, W, \alpha_0, \Gamma$ given above, the corresponding values of $\lambda = 3.5, 0.35$ and the relative density difference $\epsilon = -0.02857, -0.2857$ for the two cases respectively were obtained from the definitions (3.29) and (3.32). The Rossby number of the flow, $Ro = |\epsilon|$, was thus a factor ten larger in the second case.

The first case, $\Gamma = 0.2$, is presented in figures 8 and 9 and also figures 5 and 6. The stratification of the mixture is apparent in figure 8 which shows contours of constant concentration of both the numerical and the analytical solution. Away from the region of the clear fluid–suspension interface the two solutions are almost indistinguishable. Deviations appeared mainly due to the artificial smearing of the numerical solution around the shock. Figure 9 shows the numerical result for the azimuthal velocity in the form of isovelocity lines. The position of the shock is immediately recognized as the diagonal band of rapidly changing velocity in the right half of this graph. Above the interface the velocity is negative and more or less independent of z whereas below the interface it is positive and decreasing towards the inlet as an effect of the continuous stratification. The velocity change crossing the shock in the positive axial direction is thus negative, reflecting the rapid density increase there, whereas in the mixture the velocity increases as an effect of the reversed density change in that region. At smaller radii there is no clear fluid present and away from the Ekman layers the azimuthal velocity increases monotonically in the axial direction. However, the velocity is negative in most of the cylinder and changes to positive only rather close to the outlet.

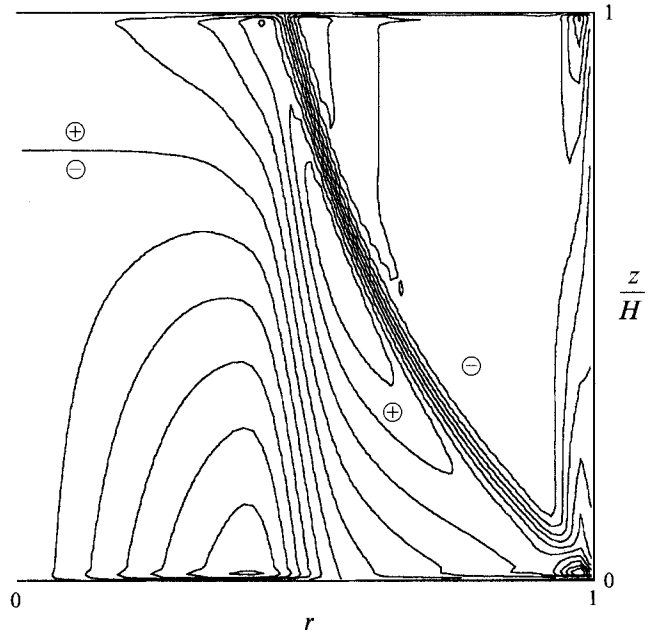

FIGURE 9. Lines of constant azimuthal velocity in a meridional plane of the numerical solution for the same case as in figure 8; $\Gamma = 0.2$, $v = -0.024 + i \times 0.004$, $i = 0, 1, \ldots, 13$.

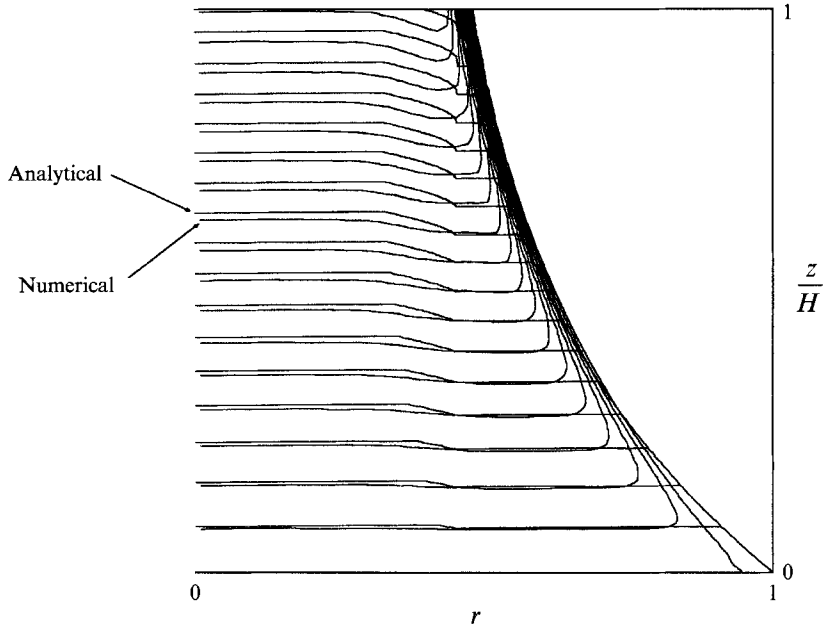

FIGURE 10. Comparison between analytical and numerical solution of iso-concentration lines in a meridional plane; $\Gamma = 2.0$, $E = 0.25 \times 10^{-4}$, $W = 0.7$, $\alpha_0 = 0.05$, $\beta = 0.05$. $\alpha = 0.05 + i \times 0.01$, $i = 0, 1, \ldots, 18$.

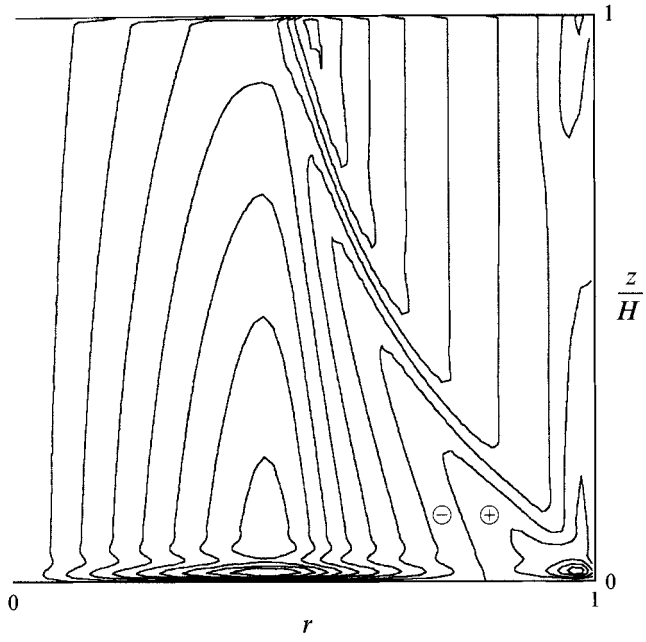

FIGURE 11. Lines of constant azimuthal velocity in a meridional plane of the numerical solution for the same case as in figure 10; $\Gamma = 2.0$. $v = -0.081 + i \times 0.009$, $i = 0, 1, \ldots, 13$.

The adjustment to the no-slip conditions can be observed as Ekman layers at the in- and outlet and as a vertical shear layer at the vertical wall. A free vertical shear layer is also observed in the transition region between the differentially rotating fluid below the interface and in the inner part of the cylinder. An order of magnitude estimate of the thickness of the vertical layers would be $\sim E^{\frac{1}{4}} = 0.07$ which seems to be roughly in agreement with those in the graph. Comparisons of the numerical solution and a vertically uniformly valid composite solution of the interior and boundary layer solutions of the asymptotic analysis are shown by the upper curves in figures 5 and 6 for $r = 0.15$ and 0.66 (where for comparison $r_{sh} \approx 0.47$). The calculation of the analytical velocity profile in the interior according to (3.11) was here evaluated with the concentration field corrected to first order in $E^{\frac{1}{2}}$. The agreement is generally very good. For $r = 0.15$ there is a small shift of the analytical curve to smaller negative values of v whereas the slope is more or less identical. At $r = 0.66$ the curves collapse everywhere except in the transition region of the shock where no Ekman layer is present in the numerical solution due to the artificial smearing of the concentration field.

The second case, $\Gamma = 2.0$, is presented in figures 10 and 11 and also figures 5 and 6. Concentration contours are shown in figure 10. As expected the graph is similar to the first case. However, radial variations also appear in the mixture region away from the interface. Following the flow from the inlet a concentration difference develops between the inner part of the cylinder and the region below the interface. The transition between these two differentially stratified areas appears as a smooth radial density gradient. The corrections added to the analytical solution due to the secondary circulation and the modified centrifugal force on the particles seem to catch the basic features of the numerical solution, including the width of the transition region. The azimuthal velocity is presented in figure 11. The magnitude of the azimuthal velocity is now larger and in the negative azimuthal direction in most of the cylinder except for a small region in the lower right corner of the graph in figure 11. Generally the larger

magnitude of v is expected in order to allow the Ekman layer flows to compensate for the increased mass flux in the core. Owing to the effect of axial convection, the Ekman layers at the in and outlet are now of completely different character. The Ekman layer at the inlet is thicker, with clear oscillations whereas at the outlet the boundary layer-thickness is definitely smaller. This is also clear from the lower curves in figures 5 and 6 which show a comparison of the azimuthal velocity profiles between the analytical and numerical solutions at $r = 0.15$ and 0.66 for the second case. As could be expected for a larger value of $Ro = |\epsilon|$ the differences between the analytical and numerical solutions are slightly larger than in the first case. The agreement appears closer at $r = 0.66 > r_{sh}$ than at $r = 0.15 < r_{sh}$ which might be surprising since the secondary Ekman layer flux balance is more complex in the outer region and the numerical solution does not reproduce the Ekman layers at the clear fluid–suspension interface. However, if a relative measure of the discrepancy is used the agreement is slightly closer at $r = 0.15$.

6. Conclusions

We have considered continuous centrifugal separation of a two-phase mixture flowing axially through a circular cylinder. An approximate analytical solution valid for asymptotically small values of the Ekman and Rossby numbers has been presented and compared with the results from a numerical computation.

Separation of the phases manifested itself as both continuous and discontinuous stratifications in the cylinder. For light particles heavy clear fluid appeared in a region adjacent to the outer rim of the cylinder on top of the lighter mixture. The shape of the interface separating the two fluid regions reflected the trajectory of an axially advected, sedimenting particle in the mixture originating at the outer rim of the inlet. Within the mixture region itself the density decreased continuously in the axial direction as an effect of the gradual packing of (light) particles in the axially advected mixture. For a uniform axial inlet velocity profile the density gradient within the mixture was approximately aligned with the rotation axis in the parameter regime considered.

A clear physical picture of the flow field was obtained from the asymptotic analysis. In analogy with thermal winds in the Earth's atmosphere buoyancy from the stratifications in the cylinder, balanced by the Coriolis acceleration, induced an azimuthal swirl velocity of the fluid. The positive density jump at the clear fluid–suspension interface thus induced a negative azimuthal velocity jump and the downward density gradient in the mixture required a positive gradient of the azimuthal velocity. Ekman layers appeared at the horizontal in- and outlets where no-slip conditions were imposed for the tangential velocity components. The radial mass fluxes in the Ekman layers were crucially dependent on the ratio of the axial velocity and the Ekman-layer diffusion velocity, $\Gamma \equiv w^*_{in}/(\Omega \nu^*_C)^{\frac{1}{2}}$. It was shown that for increasing values of Γ the relative mass transport efficiency increased at Ekman layers with injection of fluid whereas suction of fluid had the opposite effect.

Secondary circulations in meridional planes of the inviscid interior appeared due to both the separation and the Ekman-layer pumping. An inward radial mass flow, $\sim E^{\frac{1}{2}}\Gamma$, compensated the total angular momentum of a mixture fluid element for the axially increasing azimuthal velocity through the cylinder. This radial flow forced fluid towards the horizontal boundaries where fluid sucked into the Ekman layers was redirected outwards. The outward phase-averaged mass transport of the separation process thus appeared only within the Ekman layers.

To obtain the net outward Ekman-layer flux necessary to balance the secondary radial interior flow, i.e. to fulfil the global volumeflux requirements, a retrograde

intensification of the azimuthal velocity was required for increasing values of Γ. Thus, at the bottom Ekman layer, where fluid was injected from the boundary, an increased outward mass flux was allowed for increasing values of this parameter whereas at the top boundary suction of fluid diminished the mass flux in the Ekman layer.

The numerical computation qualitatively confirmed the physical picture described above. Typical for the numerical solution was a small departure from a strictly axial stratification. It was found that this could be explained by the presence of the secondary circulation and the non-uniform effective centrifugal force on the particles due to the flow in the dynamically different regions of the mixture core and the mixture below the clear fluid region. Two cases were compared with the results from the asymptotic analysis with $\Gamma = 0.2$ and $\Gamma = 2.0$ respectively, which confirmed the crucial dependence of the solution on Γ. The quantitative agreement away from the vertical shear layers was very good in both cases, except at the position of the clear fluid–suspension interface where the kinematic shock of the asymptotic analysis was smeared out in the numerical solution to a continuous variation of the particle concentration by the introduction of artificial diffusion of particles. Therefore no true Ekman layers were observed in the numerical solution at the interface. Though the Ekman-layer flux balance was found to be very important in the asymptotic analysis, the lack of these particular boundary layers was of no consequence for the good agreement away from the interface. In all, the numerical results gave confidence in further use of the code.

In summary the most important results obtained were:

(i) an analytical solution based on 'mixture theory' of a canonical flow case for continuous separation;

(ii) a linear Ekman-layer solution for boundaries with axial injection or suction;

(iii) a successful verification of a numerical code for mixture theory including the effects of phase-averaged mass flow divergence which are typical for centrifugally separating mixtures.

An unanswered question is the stability properties of the flow. The Ekman layers with injection at the boundary are likely to be more unstable than ordinary Ekman layers. There is also a potential for baroclinic instability of the azimuthal flow in the stratified mixture, a topic which was not considered in this work.

Appendix A. The Ekman-layer solution

We consider Ekman-layer flow at a surface $z = Z(r)$, which could represent either of the horizontal boundaries at $z = 0$ and $z = H$ or the position of the kinematic shock at $z = \Sigma(r)$, with an axial flow injected at the surface according to the inviscid outer flow. Let the upward pointing unit normal from the surface be $\boldsymbol{l}$ and let the stretched boundary-layer coordinate along this normal be ζ where the non-dimensional distance from the surface is $E^{\frac{1}{2}}\zeta$. At the Ekman layer at $z = 0$ and at the upper side of the shock at $z = \Sigma(r)$ we thus have $\zeta > 0$ with injection of fluid at the surface whereas at $z = H$ and on the lower side of the shock we have $\zeta < 0$ and suction of fluid. The boundary-layer solution $(\boldsymbol{q}_E, \alpha_E, P_E)$ is expressed in terms of a correction to the outer inviscid flow:

$$\boldsymbol{q}_E = \boldsymbol{q}(r,z) + \boldsymbol{q}_i(r,\zeta), \quad \alpha_E = \alpha(r,z) + \alpha_i(r,\zeta), \quad P_E = P(r) + P_i(r,\zeta), \tag{A 1}$$

where $(\boldsymbol{q}, \alpha, P)$ is the inviscid outer solution and $(\boldsymbol{q}_i, \alpha_i, P_i)$ is the inner boundary-layer correction. It follows from evaluation of the rate of change of the particle volume fraction along the short characteristic path within the Ekman layer that the boundary-layer correction to the concentration is small, $\alpha_i = O(E^{\frac{1}{2}})$, i.e. of the order of the

boundary-layer thickness. The equations for momentum balance and continuity of the mixture to zeroth order after subtracting the corresponding inviscid equations then yield

$$c\boldsymbol{l}\cdot(\boldsymbol{q}^0_\pm+\boldsymbol{q}^0_i)\frac{\partial}{\partial\zeta}\boldsymbol{q}^0_i+2\boldsymbol{e}_z\times\boldsymbol{q}^0_i=-\boldsymbol{l}\frac{\partial}{\partial\zeta}P^1_i+\mu(\alpha^0_\pm)\frac{\partial^2}{\partial\zeta^2}\boldsymbol{q}^0_i, \tag{A 2}$$

$$\frac{\partial}{\partial\zeta}\boldsymbol{l}\cdot\boldsymbol{q}^0_i=0, \tag{A 3}$$

where subscript $\pm$ denotes evaluation at the upper or lower side of the surface $z=Z(r)$. Since the boundary-layer corrections approach zero as $|\zeta|\to\infty$ we obtain

$$\boldsymbol{l}\cdot\boldsymbol{q}^0_i=0. \tag{A 4}$$

The zeroth-order boundary-layer correction for the pressure is also zero. The first-order correction P^1_i that appears in (A 2) could be eliminated using (A 4). For convenience, with $\mathrm{i}=\sqrt{-1}$, we define the complex vector

$$\boldsymbol{Q}_i=\boldsymbol{l}\times\boldsymbol{q}^0_i-\mathrm{i}\boldsymbol{q}^0_i \tag{A 5}$$

to represent the velocity components tangential to the surface, which by (A 2) yield

$$\mu(\alpha^0_\pm)\frac{\partial^2}{\partial\zeta^2}\boldsymbol{Q}_i-\boldsymbol{l}\cdot\boldsymbol{e}_z\Gamma(r)\frac{\partial}{\partial\zeta}\boldsymbol{Q}_i+2\mathrm{i}\boldsymbol{l}\cdot\boldsymbol{e}_z\boldsymbol{Q}_i=0 \tag{A 6}$$

with the outer inviscid solution substituted according to (3.10) and (3.13). The second term in (A 6) is due to the axial flow through the boundary layer and represents convection of tangential momentum in the normal direction. The strength of this convection is given by Γ which in dimensional quantities can be written

$$\Gamma\equiv w^*_{in}(r)/(\Omega^*\nu^*_0)^{\frac{1}{2}}, \tag{A 7}$$

which is the ratio of the injection velocity and the Ekman-layer viscous diffusion velocity. The general solution to (A 6) is

$$\boldsymbol{Q}_i=\boldsymbol{U}_\pm\exp\left[\mp\frac{\zeta}{\mu^{\frac{1}{2}}_\pm}\gamma\left(\frac{\pm\Gamma}{\mu^{\frac{1}{2}}_\pm};\boldsymbol{l}\right)\right], \tag{A 8}$$

where the upper/lower index or sign holds if $\zeta>0/\zeta<0$. γ is a complex function that is defined for brevity as

$$\gamma(x;\boldsymbol{l})=-\tfrac{1}{2}x\boldsymbol{l}\cdot\boldsymbol{e}_z+(1-\mathrm{i})(\boldsymbol{l}\cdot\boldsymbol{e}_z+\mathrm{i}(\boldsymbol{l}\cdot\boldsymbol{e}_z)^2x^2/8)^{\frac{1}{2}}. \tag{A 9}$$

At $\zeta=0$, i.e. at the surface in question, the sum of the interior velocity and the boundary-layer correction have to equal the actual fluid velocity at the surface, $\boldsymbol{u}$ say, so that

$$\boldsymbol{U}_\pm=-[\boldsymbol{l}\times(\boldsymbol{q}^0_\pm-\boldsymbol{u})-\mathrm{i}(\boldsymbol{q}^0_\pm-\boldsymbol{u})], \tag{A 10}$$

which completes the zeroth-order solution.

To first order in $E^{\frac{1}{2}}$ the Ekman-layer continuity equation implies

$$\frac{\partial}{\partial\zeta}\boldsymbol{l}\cdot\boldsymbol{q}^1_i+\boldsymbol{l}\cdot\boldsymbol{\nabla}\times(\boldsymbol{l}\times\boldsymbol{q}^0_i)=0. \tag{A 11}$$

On substituting the Ekman-layer solution (A 8), (A 11) can be integrated to give

$$\boldsymbol{l}\cdot\boldsymbol{q}^1_i(\zeta)=\pm\boldsymbol{l}\cdot\boldsymbol{\nabla}\times\left[Re\left\{\boldsymbol{Q}_i(\zeta)\mu^{\frac{1}{2}}_\pm/\gamma\left(\frac{\pm\Gamma}{\mu^{\frac{1}{2}}_\pm};\boldsymbol{l}\right)\right\}\right], \tag{A 12}$$

from which the Ekman-layer pumping velocities are obtained for $\zeta\to0$.

Appendix B. Derivation of compatibility conditions

We consider first matching of the outer inviscid solution to the inner solution of the Ekman layers at the horizontal boundaries which requires

$$w(z = 0/H) + w_i(\zeta = 0) = w_{in}. \tag{B 1}$$

As for zeroth order $w^0 = w_{in}$ we obtain to first order

$$w_1(z = 0/H) + w_i^1(\zeta = 0) = 0. \tag{B 2}$$

It then follows from (B 2), (A 12), (A 8) and (A 10) with $\boldsymbol{l} = \boldsymbol{e}_z$ that

$$\begin{aligned} \boldsymbol{e}_z \cdot \boldsymbol{q}_i^1(z = 0/H) &= w_i^1(\zeta = 0) \\ &= \pm \boldsymbol{e}_z \cdot \boldsymbol{\nabla} \times \left[Re \left\{ [\boldsymbol{e}_z \times (\boldsymbol{q}^0 - \boldsymbol{u}) - \mathrm{i}(\boldsymbol{q}^0 - \boldsymbol{u})] (\mu_{0/H})^{\frac{1}{2}} / \gamma \left(\frac{\pm \Gamma}{(\mu_{0/H})^{\frac{1}{2}}}; \boldsymbol{e}_z \right) \right\} \right]_{z=0/H}, \end{aligned} \tag{B 3}$$

where $\boldsymbol{u} = w_{in} \boldsymbol{e}_z$. Evaluation of (B 3) directly yields (3.33) and (3.34).

At the clear fluid–suspension interface the compatibility relation for the inviscid mass-averaged velocity is derived from the first-order expansion for the shock condition (2.21*f*). With (3.13) and (3.29), (2.21*f*) to first order gives

$$[\boldsymbol{q}^1 \cdot \boldsymbol{n}]_-^+ + [\boldsymbol{q}_i^1 \cdot \boldsymbol{n}]_-^+ = -s \frac{W}{\lambda} \boldsymbol{n} \cdot \boldsymbol{e}_z [\alpha^0]_-^+. \tag{B 4}$$

For the inviscid solution in the first term of (B 4) we get, with (2.20),

$$[\boldsymbol{q}^1 \cdot \boldsymbol{n}]_-^+ = \boldsymbol{n} \cdot \boldsymbol{e}_z ([w^1]_-^+ - \Sigma'(r)[u^1]_-^+). \tag{B 5}$$

The first-order radial component is taken from (3.31 *b*) and the difference in (B 5) rewritten with help of (3.18) which gives

$$\Sigma'(r)[u^1]_-^+ = -s \frac{W}{2\lambda} [\alpha^0]_-^+. \tag{B 6}$$

For the second term in (B 4) the first-order boundary-layer corrections on both sides of the shock are obtained from (A 12) at $\zeta = 0$. The integration constants $\boldsymbol{U}_\pm$ are then chosen such that the velocity and shear stresses tangential to the interface of the zeroth-order interior solutions are continuous there according to (2.21*a*) and (2.21*e*). The Ekman pumping in the direction normal to the shock then yields

$$[\boldsymbol{q}_i^1 \cdot \boldsymbol{n}]_-^+ = \boldsymbol{n} \cdot \boldsymbol{\nabla} \times \left(\frac{W}{2\lambda} [\boldsymbol{q}^0]_-^+ \right)_{z=\Sigma(r)} \tag{B 7}$$

The final expression (3.36), quantifying the jump of the first-order inviscid vertical velocity component across the shock, is obtained after substitution of (B 7) and (B 5) with (B 6) into (B 4).

Appendix C. Expressions for the functions $G(r)$ and $D(r)$

The integral of the volume flux requirement (3.37) can be subdivided into the contributions from the inviscid interior and the Ekman layers respectively:

$$J_r = E^{\frac{1}{2}} 2\pi r \left(\int_0^H j_r^1 \, \mathrm{d}z + \sum_n \int \boldsymbol{q}_E^0 \cdot \boldsymbol{e}_\theta \times \boldsymbol{l}_n \, \mathrm{d}\zeta \right) = 0, \tag{C 1}$$

where summation is applied over all the Ekman layers present at the radial position in question. For the interior contribution to lowest order the integral yields

$$J_I = 2\pi r \int_0^H j_r^1 \,\mathrm{d}z = 2\pi r \int_0^H 3u^1 \,\mathrm{d}z = 2\pi r^2 \int_0^H s\tfrac{3}{4} \frac{W}{\lambda} \frac{\mathrm{d}}{\mathrm{d}z} \alpha^0 \,\mathrm{d}z, \tag{C 2}$$

where (2.8), (3.15*a*) and (3.26) are used. Integration gives, with $s = -1$,

$$J_I = \begin{cases} \dfrac{3W}{2\lambda} \pi r^2 [\alpha_0 - \alpha^0(z = H)] & \text{for} \quad r \leqslant r_{sh} \\ \dfrac{3W}{2\lambda} \pi r^2 [\alpha_0 - \alpha^-(r)] & \text{for} \quad r \geqslant r_{sh}. \end{cases} \tag{C 3}$$

For the various boundary layers we obtain

$$J_E(z = 0) = -\pi r [\mu(\alpha_0)]^{\frac{1}{2}} v^0(z = 0, r)\, B_0, \tag{C 4}$$

$$J_E(z = H) = \begin{cases} -\pi r [\mu(\alpha_H^0)]^{\frac{1}{2}} v^0(z = H, r)\, B_H & \text{for} \quad r < r_{sh} \\ -\pi r v^0(z = H, r)\, B[\gamma(-\Gamma, \boldsymbol{e}_z]) & \text{for} \quad r > r_{sh}, \end{cases} \tag{C 5}$$

$$J_E(z = \Sigma(r)) = -\pi r \frac{W}{\lambda} [v^0]_-^+ = -s\pi r^2 \frac{W}{2\lambda} \alpha^-(r) = \pi \frac{W}{2\lambda} \alpha_0, \tag{C 6}$$

where subscripts 0 and H denote evaluation with the same argument as used in (3.33) and (3.34) respectively. It can be observed that $J_E(z = \Sigma(r))$ is non-divergent, from which it follows that $D^+ = D^-$. The full expressions for $G(r)$ and $D(r)$ obtained from the boundary conditions and the volume flux requirements are given below.

The functions appearing in the expressions for the inviscid asymptotic solution are

$$G(r) = \begin{cases} r(-\alpha_0 + (\alpha_0 - \alpha_H)\, k_1), & r < r_{sh} \\ -r\alpha_0 k_2 + k_3/r, & r > r_{sh}, \end{cases} \tag{C 7}$$

$$D(r) = \begin{cases} -\alpha_0\, 3W/2\lambda + \tfrac{1}{2}(\alpha_0 - \alpha_H)\, (\mu(\alpha_0))^{\frac{1}{2}} B_0 k_1, & r < r_{sh} \\ \tfrac{1}{2}\alpha_0 B_C k_2, & r > r_{sh}, \end{cases} \tag{C 8}$$

where

$$k_1 = \frac{(\mu(\alpha_H))^{\frac{1}{2}} B_H + 3W/\lambda}{(\mu(\alpha_H))^{\frac{1}{2}} B_H + (\mu(\alpha_0))^{\frac{1}{2}} B_0}, \tag{C 9}$$

$$k_2 = \frac{(\mu(\alpha_0))^{\frac{1}{2}} B_0 - 3W/\lambda}{(\mu(\alpha_0))^{\frac{1}{2}} B_0 + B_C}, \quad k_3 = \frac{-2\alpha_0 W/\lambda}{(\mu(\alpha_0))^{\frac{1}{2}} B_0 + B_C}, \tag{C 10), (C 11}$$

$$B_0 = B\left[\gamma\left(\frac{\Gamma}{(\mu(\alpha_0))^{\frac{1}{2}}}; \boldsymbol{e}_z\right)\right], \quad B_H = B\left[\gamma\left(\frac{-\Gamma}{(\mu(\alpha_H))^{\frac{1}{2}}}; \boldsymbol{e}_z\right)\right], \quad B_C = B[\gamma(-\Gamma; \boldsymbol{e}_z)] \tag{C 12)–(C 14}$$

and where α_0 is the inlet concentration, $\alpha_H = \alpha^0(z = H)$ and γ is defined by (A 9) in Appendix A.

REFERENCES

AMBERG, G., DAHLKILD, A. A., BARK, F. H. & HENNINGSON, D. S. 1986 On time-dependent settling of a dilute suspension in a rotating conical channel. *J. Fluid Mech.* **166**, 473–502.

AMBERG, G. & GREENSPAN, H. P. 1987 Boundary layers in a sectioned centrifuge. *J. Fluid Mech.* **181**, 77–97.

AMBERG, G. & UNGARISH, M. 1993 Spin-up from rest of a mixture: simulation and theory. *J. Fluid Mech.* **246**, 443–464.

DAHLKILD, A. A., AMBERG, G. & GREENSPAN, H. P. 1992 Flow in a centrifugal spectrometer. *J. Fluid Mech.* **238**, 221–250.

DAHLKILD, A. A. & GREENSPAN, H. P. 1989 On the flow of a rotating mixture in a sectioned cylinder. *J. Fluid Mech.* **198**, 155–175.

GOLDSHTIK, M. A. & JAVORSKY, N. I. 1989 On the flow between a porous rotating disk and a plane. *J. Fluid Mech.* **207**, 1–28.

GREENSPAN, H. P. 1983 On centrifugal separation of a mixture. *J. Fluid Mech.* **127**, 91–101.

GREENSPAN, H. P. 1988 On the vorticity of a rotating mixture. *J. Fluid Mech.* **191**, 517–528.

GREENSPAN, H. P. & UNGARISH, M. 1985*a* On the centrifugal separation of a bulk mixture. *Intl J. Multiphase flow* **11**, 825–836.

GREENSPAN, H. P. & UNGARISH, M. 1985*b* On the enhancement of centrifugal separation. *J. Fluid Mech.* **157**, 359–373.

ISHII, M. 1975 *Thermo-Fluid Dynamic Theory of Two-Phase Flow.* Paris: Eyrolles.

KAN, J. VAN 1986 A second order accurate pressure-correction scheme for viscous incompressible flow. *SIAM J. Sci. Comput.* **7**, 870–891.

KÁRMÁN, T. VON 1921 Über laminare und turbulente Reibung. *Z. Angew. Math. Mech.* **1**, 233–251.

LEIGHTON, D. & ACRIVOS, A. 1987*a* Measurement of shear-induced self-diffusion in concentrated suspensions of spheres. *J. Fluid Mech.* **177**, 109–131.

LEIGHTON, D. & ACRIVOS, A. 1987*b* The shear-induced migration of particles in concentrated suspensions. *J. Fluid Mech.* **181**, 415–439.

NIR, A. & ACRIVOS, A. 1990 Sedimentation and sediment flow on inclined surfaces. *J. Fluid Mech.* **212**, 139–153.

PHILLIPS, R. J., ARMSTRONG, R. C. & BROWN, R. A. 1992 A constitutive equation for concentrated suspensions that accounts for shear-induced particle migration. *Phys. Fluids* A **4**, 30–40.

ROGERS, M. H. & LANCE, G. N. 1960 The rotationally symmetric flow of a viscous fluid in the presence of an infinite rotating disk. *J. Fluid Mech.* **7**, 617–631.

SCHAFLINGER, U. 1987 Enhanced centrifugal separation with finite Rossby numbers in cylinders with compartment walls. *Chem. Engng Sci.* **42**, 1197.

SCHAFLINGER, U. 1990 Centrifugal separation of a mixture. *Fluid Dyn. Res.* **6**, 213–249.

SCHAFLINGER, U., KÖPPL, A. & FILIPCZAK, G. 1986 Sedimentation in cylindrical centrifuges with compartments. *Ing. Arch.* **56**, 321.

SCHAFLINGER, U. & STIBI, H. 1987 On centrifugal separation of suspensions in cylindrical vessels. *Acta Mechanica* **67**, 163–181.

STUART, J. T. 1954 On the effects of uniform suction on the steady flow due to a rotating disk. *Q. J. Mech. Appl. Maths* **VII**.

UNGARISH, M. 1986 Flow of a separating mixture in a rotating cylinder. *Phys. Fluids* **29**, 640–646.

UNGARISH, M. 1988*a* Two fluid analysis of centrifugal separation in a finite cylinder. *Intl J. Multiphase Flow* **14**, 233–243.

UNGARISH, M. 1988*b* On shear layers in a mixture separation within inclined rotating containers. *J. Fluid Mech.* **193**, 27–51.

UNGARISH, M. 1990 Spin-up from rest of a mixture. *Phys. Fluids* A **2**, 160–166.

UNGARISH, M. 1991 Spin-up from rest of a light-particle suspension in a cylinder: Theory and observations. *Intl J. Multiphase flow* **17**, 131–143.

UNGARISH, M. 1993 *Hydrodynamics of Suspensions: Fundamentals of Centrifugal and Gravity Separation.* Springer.